5711

Computational fluid dynamics in ventilation

H B AWBI, PhD, MIMechE, MCIBSE, MRAeS and G GAN, PhD
Department of Construction Management and Engineering
University of Reading, UK

SYNOPSIS Results from a CFD program which has been developed for simulating air flow in buildings are presented. The program uses the finite volume method to solve in three-dimensions the Navier-Stokes equation, the enthalpy equation, the concentration of species equation, the equations for turbulence energy and its dissipation, the radiant heat transfer equation and the thermal comfort equation. Simulation and experimental data are presented for an air conditioned office module, a down-flow clean room and a naturally ventilated classroom.

1 INTRODUCTION

The prediction of air movement in spaces is one of the most challenging tasks for the designer of HVAC systems. The success of any such system is ultimately measured by the building user who is directly influenced by the air movement pattern in the space. A recent study by Fanger et al (1) has highlighted the effect of air movement on human thermal comfort. It has shown that human sensation of draught is due to the relative air velocity of the air as well as its turbulence intensity.

The drive for energy efficiency in buildings which started some eighteen years ago has resulted into a building stock which is better thermally insulated than before and more airtight. Consequently, more and more commercial, industrial and public buildings are being equipped with mechanical ventilation or air-conditioning systems. The need for accurate prediction of the air flow in occupied spaces has become even more crucial because, with mechanical ventilation, large quantities of air have to be evenly distributed in the space being ventilated. Without adequate air distribution, excessive air movement (draught) can occur in some zones whereas stagnant air may be present in other zones of the same room. Poor air distribution can degrade the quality of indoor air either by inadequate supply of outdoor air to the occupants or by the ineffectiveness of the supply air in removing or diluting odours and other contaminants produced within the room. Low outdoor air supply rates and high contaminant concentrations indoors are recipes for the sick building syndrome (2). In cleanrooms which are used for manufacturing delicate electronic components or pharmaceutical products higher concentration levels of contaminants or particulates can significantly influence the quality of such products.

Until recently the air movement in a space was predicted from air jet diffusion data and/or testing a physical model of the whole enclosure or a module if it is too large as described by Awbi (3). In physical modelling scale effects can be very significant particularly when dealing with buoyant flows (4). With the almost exponential increase in computing power over the last decade it is now feasible to predict the air flow in buildings by solving the full Navier-Stokes equations in three dimensions. Advances in turbulence modelling and computational schemes have accelerated the application of computational fluid dynamics (CFD) to the design of ventilation systems. A review of recent applications of CFD in room air movement is given by Awbi (3).

In this paper a three-dimensional finite volume CFD program called ARIA-R (5) which has been developed by the authors is used for predicting the air flow in a typical air conditioned office module, a cleanroom and a naturally ventilated classroom. These cases have been selected because of the availability of some experimental data for comparison and also because they cover diverse applications.

2 FIELD EQUATIONS

2.1 Flow Equations

The general transport equation for steady, incompressible and turbulent flow of air in a room whereby all the fluctuating entities are assigned time-mean equivalents through a turbulence model is given, in Cartesian Coordinates, by:

$$\frac{\partial}{\partial x_i}(\rho U_i \phi) = \frac{\partial}{\partial x_i}\left(\Gamma_\phi \frac{\partial \phi}{\partial x_i}\right) + S_\phi \qquad (1)$$

convection diffusion source

where the dependent variable ϕ representing the velocity components U, V and W, the temperature T, the concentration of chemical species C, and the turbulence scales used in the turbulence model. The convection and diffusion terms of equation (1) become identical for all the dependent variable if Γ_ϕ represents the diffusion coefficient for the scalar variables (T, C, etc.) and the effective viscosity μ_e for the vector variables (U, V and W). The source term S_ϕ is represented by different expressions for different variables as given in Table 1.

The turbulence model used is the k-ϵ model which is based on the Boussinesq turbulence viscosity hypothesis for isotropic turbulence and uses the kinetic energy of turbulence k and its dissipation rate ϵ as the two scales. Hence, two additional transport equations for k and ϵ need to be solved, i.e. a two-equation turbulence model.

Table 1 Source terms of the flow equations

Equation	ϕ	Γ_ϕ	S_ϕ
Continuity	1	0	0
U-momentum	U	μ_e	$-\frac{\partial p}{\partial x} + \frac{\partial}{\partial x}(\mu_e \frac{\partial U}{\partial x}) + \frac{\partial}{\partial y}(\mu_e \frac{\partial V}{\partial x}) + \frac{\partial}{\partial z}(\mu_e \frac{\partial W}{\partial x}) - \frac{2}{3}\frac{\partial}{\partial x}(\rho k)$
V-momentum	V	μ_e	$-\frac{\partial p}{\partial y} + \frac{\partial}{\partial x}(\mu_e \frac{\partial U}{\partial y}) + \frac{\partial}{\partial y}(\mu_e \frac{\partial V}{\partial y}) + \frac{\partial}{\partial z}(\mu_e \frac{\partial W}{\partial y}) - \frac{2}{3}\frac{\partial}{\partial y}(\rho k) - g(\rho - \rho_o)$
W-momentum	W	μ_e	$-\frac{\partial p}{\partial z} + \frac{\partial}{\partial x}(\mu_e \frac{\partial U}{\partial z}) + \frac{\partial}{\partial y}(\mu_e \frac{\partial V}{\partial z}) + \frac{\partial}{\partial z}(\mu_e \frac{\partial W}{\partial z}) - \frac{2}{3}\frac{\partial}{\partial y}(\rho k)$
Temperature	T	Γ_T	q/C_p
Concentration	C	Γ_c	S_c
Kinetic energy	k	Γ_k	$G_s - C_D \rho \epsilon + G_B$
Dissipation rate	ϵ	Γ_ϵ	$C_1 \frac{\epsilon}{k}(G_s + G_B) - C_2 \rho \frac{\epsilon^2}{k}$

Notes: $\mu_e = \mu + \mu_t$

$$G_s = \mu_t \{2 [(\frac{\partial U}{\partial x})^2 + (\frac{\partial V}{\partial y})^2 + (\frac{\partial W}{\partial z})^2] + (\frac{\partial U}{\partial y} + \frac{\partial V}{\partial x})^2 + (\frac{\partial U}{\partial z} + \frac{\partial W}{\partial x})^2 + (\frac{\partial V}{\partial z} + \frac{\partial W}{\partial y})^2 \}$$

= Kinetic energy generation by shear

$$G_B = \beta g \frac{\mu_t}{\sigma_t}\frac{\partial T}{\partial y} = \text{Kinetic energy generation by buoyancy}$$

q = heat production (W/m^2)
β = volumetric expansion coefficient
ρ_o = fluid density at a reference point

Empirical constants in the equations

C_μ	C_D	C_1	C_2	σ_T	σ_c	σ_k	σ_ϵ	σ_t
0.09	1.0	1.44	1.92	0.9	0.9	1.0	1.22	0.9

The diffusion coefficient, Γ_ϕ, for the scalar variables T, C, k and ϵ is given by the effective diffusion coefficient Γ_e thus:

$$\Gamma_\phi = \Gamma_e = \mu/\sigma + \mu_t/\sigma_\phi \qquad (2)$$

where μ is the molecular viscosity, $\sigma = \mu C_p/\lambda$ is the laminar Prandtl or Schmidt number (where C_p is the specific heat and λ is the thermal conductivity of the fluid), σ_ϕ is turbulent Prandtl number for variable ϕ and μ_t is the turbulent or eddy viscosity. In the k-ϵ model μ_t is given as:

$$\mu_t = C_\mu \rho k^2/\epsilon \qquad (3)$$

where ρ is the fluid density and C_μ is a constant equal 0.09. The kinetic energy of turbulence k is represented in terms of the fluctuating velocity components as follows:

$$k = \tfrac{1}{2}[(\overline{u'})^2 + (\overline{v'})^2 + (\overline{w'})^2] \qquad (4)$$

For a non-isothermal flow buoyancy terms are added to the source term S_ϕ in the equations for the vertical component of velocity V, k and ϵ to allow for the buoyancy force due to the temperature difference between the computational cell and a reference value such as the supply or extract temperature, see Table 1.

Equation (1) is discretised and solved for each variable ϕ in a staggered grid using the finite volume method and a line-by-line and then a plane-by-plane iterative procedure. A hybrid solution scheme consisting of central and upwind differencing is used for solving the discretised equations. No pressure equations are solved because the field pressure is linked to the velocity by using a staggered grid and the SIMPLE algorithm due to Patankar and Spalding (6). Wall function expressions for turbulent boundary layers are used to specify the value of ϕ at the first node point from a solid boundary. This requires the first grid point to be located in the turbulent region of the boundary layer. The iterative procedure is repeated until a converged solution is achieved which is indicated by the sum of the residues of ϕ for all the grid points being less than say 1% of the total flux at the supply openings. Further details of the solution procedure and boundary conditions used are described by Awbi (3,7).

2.2 Radiation Equations

When a heat source or sink is present in a room the heat transfer to the room air takes place by convection and to the room surfaces by radiation. The resulting change in air and surface temperatures will affect the convective heat transfer rate from the room surfaces and possibly the air movement in the room. It is, therefore, necessary to calculate the internal temperatures of room surfaces and use these as boundary values in the CFD prediction. The temperature T_i of a surface i is obtained from the radiosity J_i of the surface using the equation

$$J_i = \epsilon_i \sigma T_i^4 + (1-\epsilon_i) \sum_{j=1}^{n-1} F_{ij} J_j \qquad (5)$$

where σ is Stefan-Boltzmann's constant, ϵ_i is the emissivity of surface i, F_{ij} is the shape factor for surface i with respect to another room surface j and n is the number of room surfaces. The radiosity of a surface is the total radiant energy leaving a surface per unit time and per unit area (W/m^2). If a radiant heat flux q_i is present on surface i then the radiosity is calculated using the equation:

$$J_i = q_i + \sum_{j=1}^{n-1} F_{ij} J_j \qquad (6)$$

The emissive power from a black surface i is given by:

$$E_{bi} = J_i + \frac{1 - \epsilon_i}{\epsilon_i} q_i \qquad (7)$$

and the temperature of surface i is:

$$T_i = \sqrt[4]{(E_{bi}/\sigma)} \qquad (8)$$

2.3 Thermal Comfort Equations

According to Fanger's (8) thermal comfort criterion there are four environmental parameters and three personal parameters which interact and determine the thermal sensation of people. The environmental parameters are the air temperature, t_a, the mean radiant temperature, t_{mrt}, the relative air velocity, V_r, and the partial water vapour pressure in the air, p_a. The personal parameters are the metabolic rate, M, the work, W, and the thermal insulation of clothing, I_{cl}. In assessing the quality of the thermal environment in a room the personal parameters must be specified and the environmental parameters need to be measured or calculated. Normally the vapour pressure, p_a, is assumed to be uniform throughout the room and can be calculated from a knowledge of the relative humidity or percentage saturation. A CFD simulation based on convective heat transfer would predict the variation of air temperature and velocity within the space. However, the variation of mean radiant temperature within the space can only be calculated with the help of a radiation heat exchange model for the room.

For the calculation of t_{mrt} at any grid point in the computational domain each grid cell is considered as a rectangular parallelepiped and the plane radiant temperature, T_{prt}, at each cell surface is determined from:

$$T_{prt} = \sqrt[4]{\frac{1}{\sigma} \sum_{i=1}^{n} F_{pi} J_i} \qquad (9)$$

where F_{pi} is the shape factor from surface p of the grid cell to the visible room surface i (i = 1 to n) and J_i is the radiosity of room surface i given by equation (5). The mean radiant temperature of the grid cell is calculated as the average of the six cell surface temperatures weighted by the face area.

The predicted mean vote (PMV), which is a seven-point thermal sensation index due to Fanger (8), is calculated using:

$$\begin{aligned} PMV = {} & (0.303 \exp(-0.036\, M) + 0.028) \\ & \times \{(M - W) - 3.05 \times 10^{-3} \\ & \times [5733 - 6.99(M - W) - p_a] \\ & - 0.42\, [(M - W) - 58.15] \\ & - 1.7 \times 10^{-5}\, M\, (5867 - p_a) \\ & - 0.0014\, M(34 - t_a) \\ & - 3.96 \times 10^{-8} f_{cl} [(t_{cl} + 273)^4 - (t_{mrt} + 273)^4] \\ & - f_{cl}\, h_c\, (t_{cl} - t_a)) \end{aligned} \qquad (10)$$

where the clothing surface temperature, t_{cl}, is given as:

$$\begin{aligned} t_{cl} = {} & 35.7 - 0.028(M - W) \\ & - I_{cl} \{3.96 \times 10^{-8} f_{cl} \\ & \times [(t_{cl} + 273)^4 - (t_{mrt} + 273)^4] \\ & + f_{cl}\, h_c\, (t_{cl} - t_a)) \end{aligned} \qquad (11)$$

The convective heat transfer coefficient, h_c, takes the greater of the values given from:

$$h_c = 2.38\, (t_{cl} - t_a)^{0.25} \qquad (12)$$

for free convection

$$h_c = 12.1\sqrt{V_r} \qquad (13)$$

for forced convection

The clothing factor, f_{cl}, is directly related to the thermal resistance of clothing and is calculated from:

$$f_{cl} = 1.00 + 1.290\, I_{cl} \qquad (14)$$

for $I_{cl} \leq 0.078$ m^2K/W

$$f_{cl} = 1.05 + 0.645\, I_{cl} \qquad (15)$$

for $I_{cl} > 0.078$ m^2K/W

The predicted percentage of dissatisfied (PPD) is related to the PMV through the relationship:

$$PPD = 100 - 95 \exp[-(0.03353\, PMV^4 + 0.2179\, PMV^2)] \qquad (16)$$

3. APPLICATIONS AND DISCUSSIONS

3.1 Office Module

In recent years the air conditioning of office buildings in the U.K. has become very popular and in some cases necessary due to the expansion in the use of business machines. These machines together with artificial lighting generate a significant heat load within the space (internal gain) and air conditioning is sometimes required to offset this gain. The demand for all year air conditioning has also increased because of the tendency to build deep office spaces where internal gains are more significant than external heat gain. Most air conditioning systems for offices employ ceiling supply air terminals to utilise the ceiling surface for diffusing the air jet taking advantage of the Coanda effect. A slot diffuser is often used for supplying the air over the ceiling. A typical ceiling supply for a perimeter office module has, therefore, been selected to demonstrate the potential of CFD in room air movement prediction.

An office module of dimensions 4.9m long , 3.7m wide and 2.75m ceiling height which was subjected to detailed measurements by Jackman (9) in a laboratory mock-up has been selected for simulation. The office has a full width single-glazed window of height 1.5m. A continuous slot diffuser of slot width 20mm (7.2mm effective width) was installed on the ceiling 150mm from the curtain wall discharging air away from the window. The simulation has been carried out for two cases: one representing isothermal and cool air supply and one with warm air supply. The heat loss from the window in the heating case is 747W. The supply-room temperature difference is 5.5K and the air supply rate is 112 l/s. The air supply for the isothermal case is 120 l/s.

The CFD simulation of the air movement in the perimeter office for the isothermal case is shown in Fig. 1 as a velocity vector plot and in Fig. 2 as constant velocity contours (isovels). Figure 2 also shows measured velocities at three locations of height 0.3m above the floor and three others at a height 1.8m. The predicted isovels are in good agreement with the measured velocities. The air movement pattern depicted in Fig. 1 is typical for a unidirectional ceiling supply with isothermal flow or a cool air supply in which case the supply jet diffuses over the ceiling and deflects downwards due to the opposite wall onto the floor to form a large vortex within the room. A good mixing of supply air with room air is, therefore, achieved.

The heating results are shown in Figs. 3 to 5. The downdraught along the curtain wall caused by the cold window is clearly evident from the predicted velocity vectors and isotherms shown in Fig. 3. The flow is dominated by two triangular circulation zones; an upper zone controlled by the warm air jet and a lower zone of opposite circulation controlled by the downward buoyancy due to the cold window. The simulation results of Fig. 3 closely resemble the observed flow pattern in the test room

given in Fig. 4. The predicted isovels and temperature contours are shown in Fig. 5 with the measured velocities and temperatures at six locations also indicated on the diagram. The predicted velocity and temperature distribution in the office is very close to the measured values.

The flow pattern in the heating mode is not satisfactory because of the downdraught from the cold window and the poor mixing of primary air with room air. The resulting vertical temperature stratification can be observed in Fig. 3 and the thermal discomfort in the lower part of the occupied zone is evident from the large predicted percentage of dissatisfied (PPD) shown in Fig. 6. The recommended PPD limit by ISO is 10% (10).

3.2 Clean Room

Clean rooms are spaces where strict control of air contamination is required for quality control purposes. There are normally two types of clean rooms depending on the flow direction, viz the down-flow type and the cross-flow type. The class of a clean room represents the number of particulates of certain sizes (usually $\geq 0.5\mu m$ in diameter) that can be permitted in a unit volume of air. Down-flow clean rooms can usually produce lower contaminant concentration levels than cross-flow clean rooms. In the down-flow clean room air is supplied downward from the ceiling through HEPA filters. A CFD simulation of the flow and contaminant distribution in the down-flow clean room shown in Fig. 7 are given in Figs. 8 and 9. The clean room has four square-shape ceiling supply openings of side 0.6m and four extract openings one at each corner. The room dimensions are 4.8m x 4.8m x 2.7m ceiling height. A source of contamination generating a tracer gas of density close to that of air is placed below one supply opening at a height of 0.75m from the floor. The air supply velocity is 1m/s giving a Reynolds number based on the width of the opening of 4.2×10^4.

Murakami and Kato (11) have studied the flow in this clean room both numerically and experimentally. The experiments were carried out in a 1:6 scale model at the same Reynolds number. Because of the high change rate (83 ach) for the room the effect of buoyancy has been ignored and the simulation using ARIA-R was conducted for isothermal flow. The predicted flow pattern represented by the velocity vectors in Fig. 8 is the same as that measured by Murakami and Kato using a hot wire anemometer. The air jet from each opening descends into the room impinging onto the floor and deflecting upwards along the walls creating a recirculation zone between the jet and the wall.

The concentration contours shown in Fig. 9 have been normalised by dividing the field values by the extract concentration averaged over the four extract openings. The predicted contours are in good agreement with measurements using an ethylene (C_2H_4) source and gas chromatography particularly in the vicinity of the source. The highest concentration in the room is between the source and the floor followed by the trapped vortex region between the jet and the nearest wall. The concentration in three quarters of the room is below 0.5 because of the displacement of contamination by the three jets. The high concentration zone is limited to a quarter of the room where the source is placed.

3.3 Classroom

Natural or passive ventilation is still the most common way of ventilating buildings in the U.K. The air flow into or out of a naturally ventilated building is produced by the action of wind on the building and the effect of buoyancy caused by the temperature difference between the air inside and the air outside. Although this method of ventilation is very common in temperate climates the air flow patterns produced by natural ventilation openings have seldom been investigated. At the University of Reading the natural ventilation of classrooms and offices is currently being investigated experimentally and numerically. The air flow pattern and temperature distribution in a classroom of dimensions 10.9m x 11.0m x 3.05m ceiling height produced by cross ventilation through windows on opposite walls are shown in Fig. 10. The classroom is occupied by twenty-two people distributed over four zones (three rows of students (3 x 7) plus one lecturer). Each occupant is represented by an obstacle with 100W heat source for the purpose of air flow simulation as shown in Fig. 10. The air change rate for this case is 3.6 ach as measured by a tracer gas decay method. Figure 11 represents velocity (isovels) and temperature (isotherms) contours for a horizontal plane 0.9m above the floor which is approximately 15cm above the desks in the room. The velocities measured using omni-directional anemometers and the air temperature measured with thermocouples both at a height of 0.9m for various locations in the room are also given in Fig. 11. The figure shows that in general the predictions are in reasonable agreement with measurements, except at some points where the agreement is not very good. The latter is attributed to the assumption of air flowing into the room perpendicular to the window opening whereas in reality the flow could have been at an angle to the window opening.

More detailed description of the classroom and measurement techniques are

given by Zainal and Croome (12) and further simulations are given by Gan et al (13). The precise direction of air flow into and out of the room is almost impossible to predict because of wind turbulence.

Taking into consideration the effect of solar heat gain and internal gains the mean radiant temperature at each cell point (40 x 24 x 20 grid) is calculated and used to predict the predicted mean vote (PMV) and the predicted percentage of dissatisfied (PPD) in the classroom. The PMV and PPD contours at a height of 0.9m in the room are shown in Fig. 12. These results show a PPD in the range 5 to 14% with a mean value of 8% for the occupied zone to a height of 1.8m above the floor. Although thermal comfort standards recommend a PPD $\leq$ 10% values up to 20% may in practice be still acceptable (10).

In cold climates it may be necessary to position ventilation openings at high level in order to avoid draughts in the occupied zone. CFD can be applied to size ventilation openings in this case also and predict the air movement and comfort level in the room albeit under more critical conditions than that of the summer ventilation case presented here.

4. CONCLUSIONS

Three-dimensional CFD simulation of air movement in rooms is rapidly becoming part of the design process of ventilation systems as a result of the rapid expansion of computer power. The program described in this paper (ARIA-R) has been applied to three very different room ventilation cases with a degree of accuracy that is acceptable for most design requirements of ventilation systems. In certain cases where numerical discrepancy between measurement and prediction is evident the CFD simulation can still produce a good qualitative evaluation of the air flow. It should be said, however, that the measurement of air flow in ventilated rooms is very difficult and measurement errors can be considerable particularly when the velocities are very low.

Unfortunately, the majority of CFD software available is still complex and requires an experienced user. This is partly due to the complexity of the flow equations being solved and partly due to the physical phenomena being simulated and the simplifying assumptions that are invariably needed to achieve a solution. Because of these problems it is expected that for the foreseeable future CFD software will be restricted to the experienced user. However, considerable developments are needed to improve the predictive accuracy of CFD software such as in the areas of turbulence modelling, griding schemes, more stable solution algorithms and in prescribing boundary conditions, particularly for rooms where transitional flow can be present at some boundaries.

REFERENCES

(1) FANGER, P.O. et al. Air Turbulence and Sensation of draught, Energy and Buildings, 1988, 12, 21-39.

(2) SYKES, J.M. Sick Building Syndrome. Building Serv. Eng. Res. Technol., 1989, 10, 1-11.

(3) AWBI, H.B. Ventilation of Buildings, Spon, 1991.

(4) AWBI, H.B. and NEMRI, M.M. Scale Effect in Room Airflow Studies. Energy and Buildings, 1990, 14, 207-210.

(5) CFD Program User Manual for Airflow, Heat Transfer and Concentration in Enclosures (ARIA-R). Department of Construction Management & Engineering, University of Reading, 1991.

(6) PATANKAR, S.V. and SPALDING, D.B. A Calculation Procedure for Heat, Mass and Momentum Transfer in Three-dimensional Parabolic Flows. Int. J. Heat Mass Transfer, 1972, 15, 1787,

(7) AWBI, H.B. Application of Computational Fluid Dynamics in Room Ventilation. Building and Environment, 1989, 24, 73-84.

(8) FANGER, P.O. Thermal Comfort. McGraw-Hill, 1972.

(9) JACKMAN, P.J. Air Movement in Rooms with Ceiling-mounted Diffusers. HVRA (BSRIA) Laboratory Report No. 81, 1973.

(10) ISO 7730. Moderate Thermal Environments - Determination of the Conditions for Thermal Comfort. International Standards Organisation, 1984.

(11) MURAKAMI, S. and KATO, S. Numerical and Experimental Study on Flow and Diffusion Field in Room. Ventilation System Performance, Proc. 11th AIVC Conference, Belgirate, Italy, 1990.

(12) ZAINAL, M. and CROOME, D.J. Ventilation Characteristics of Selected Type of Buildings and Indoor Climate. Proc. 11th AIVC Conference, Belgirate, Italy, 1990.

(13) GAN, G., AWBI, H.B. and CROOME, D.J. Airflow and Thermal Comfort in Naturally Ventilated Classrooms. Proc. 12th AIVC Conference, Ottawa, Canada, September 1991.

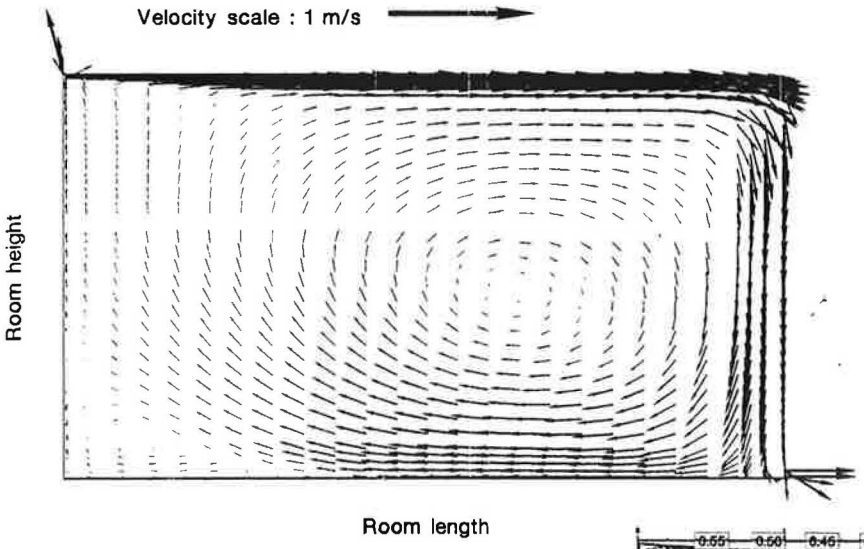

Fig 1 Predicted velocity vectors in the perimeter office for isothermal flow

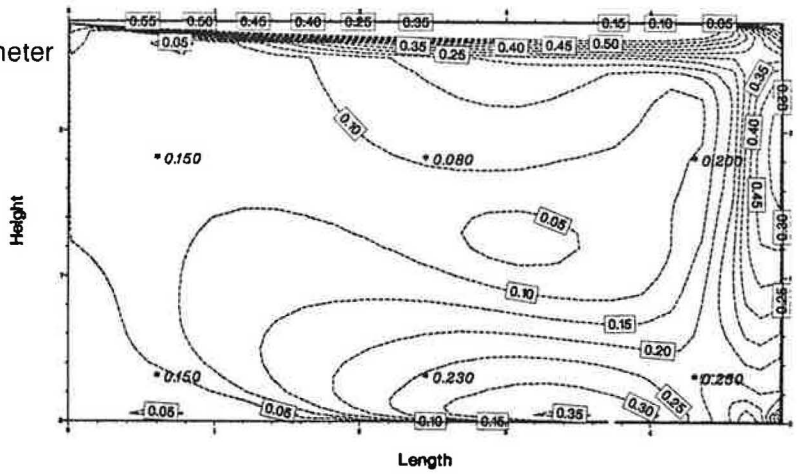

Fig 2 Comparison of predicted isovels with measured velocity (*) in the perimeter office for isothermal flow (m/s)

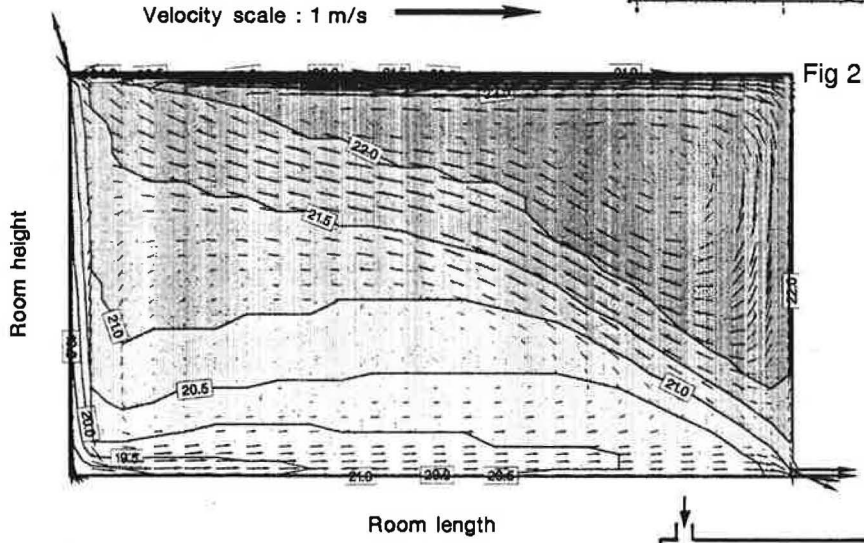

Fig 3 Predicted velocity vectors (m/s) and isotherms (°C) in the perimeter office for heating

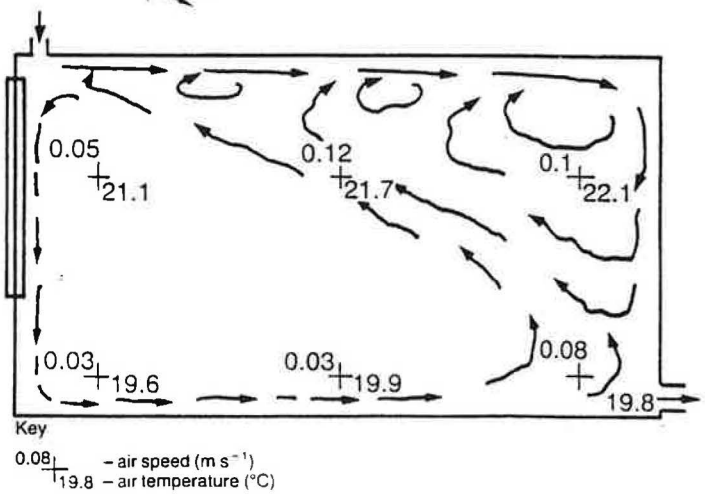

Fig 4 Observed flow pattern in the perimeter for heating

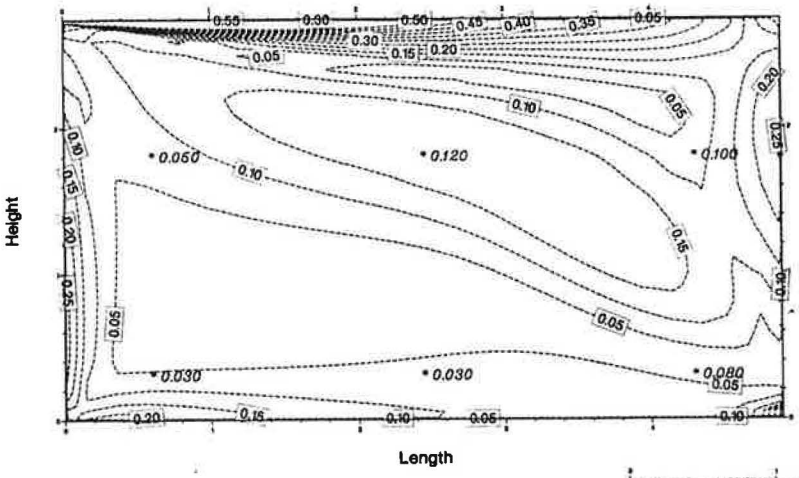

(a) Velocity (m/s)

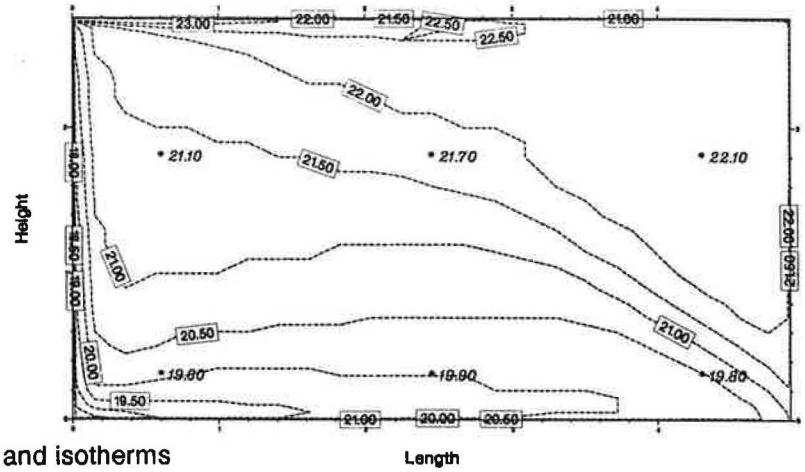

(b) Temperature (deg.C)

Fig 5 Comparison of predicted isovels and isotherms with measured velocities and temperatures (*) in the perimeter office for heating

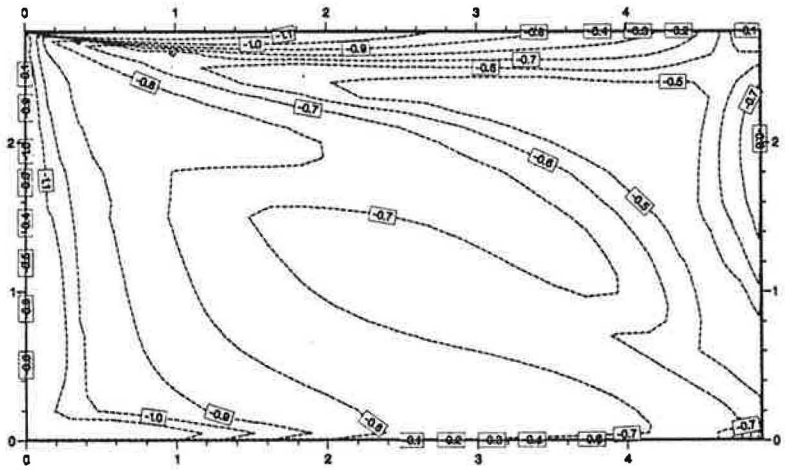

(a) Predicted mean vote

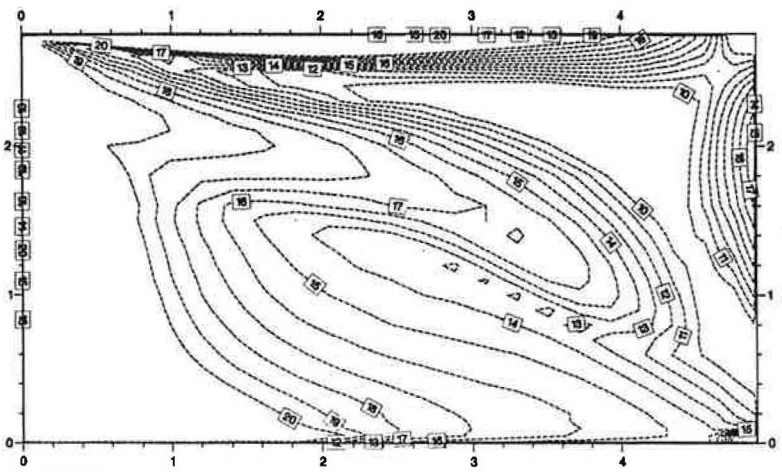

(b) Predicted percentage of dissatisfied (%)

Fig 6 Predicted mean vote and predicted percentage of dissatisfied in the perimeter office for heating

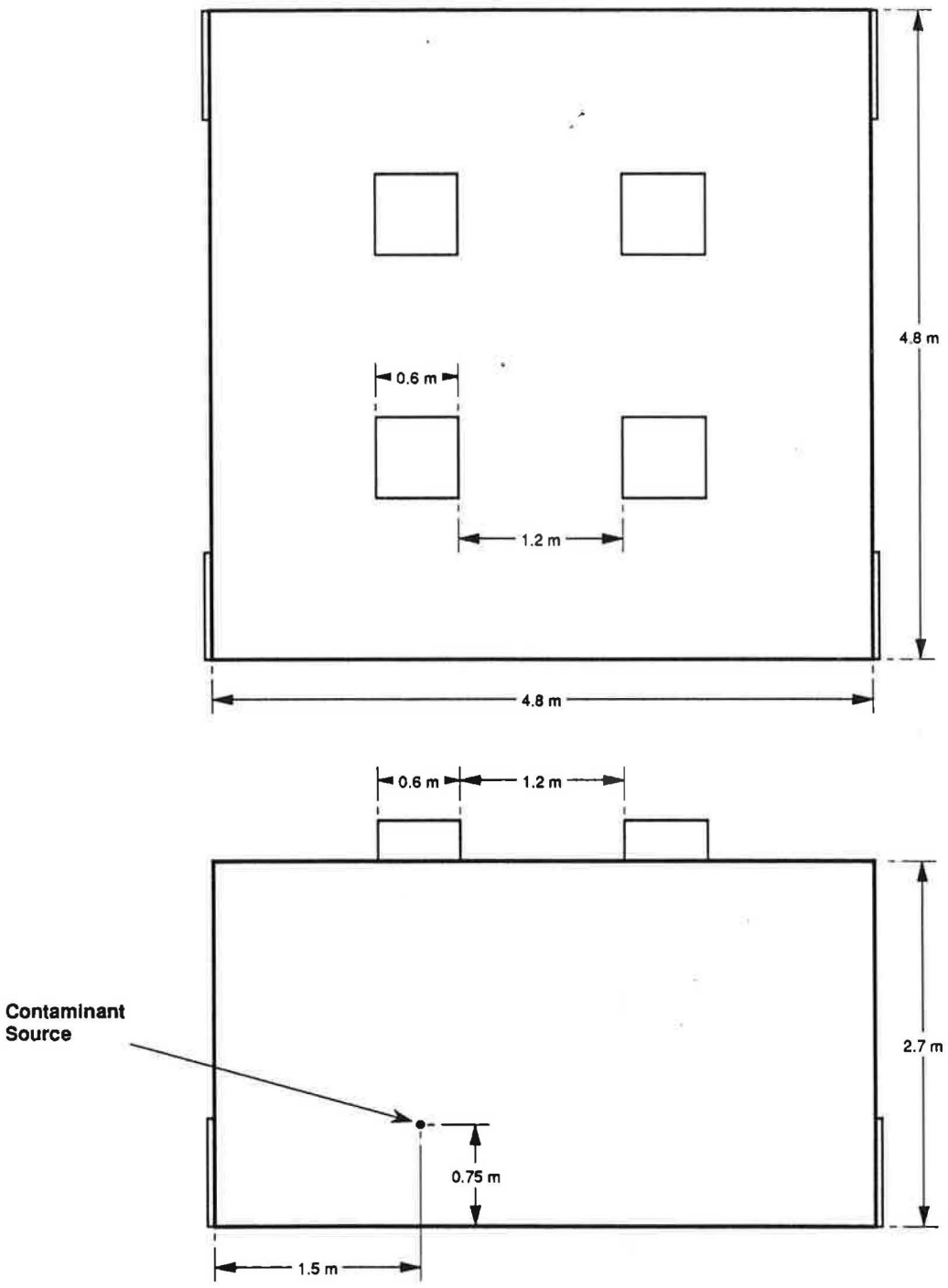

Fig 7 Plan and section of the clean room

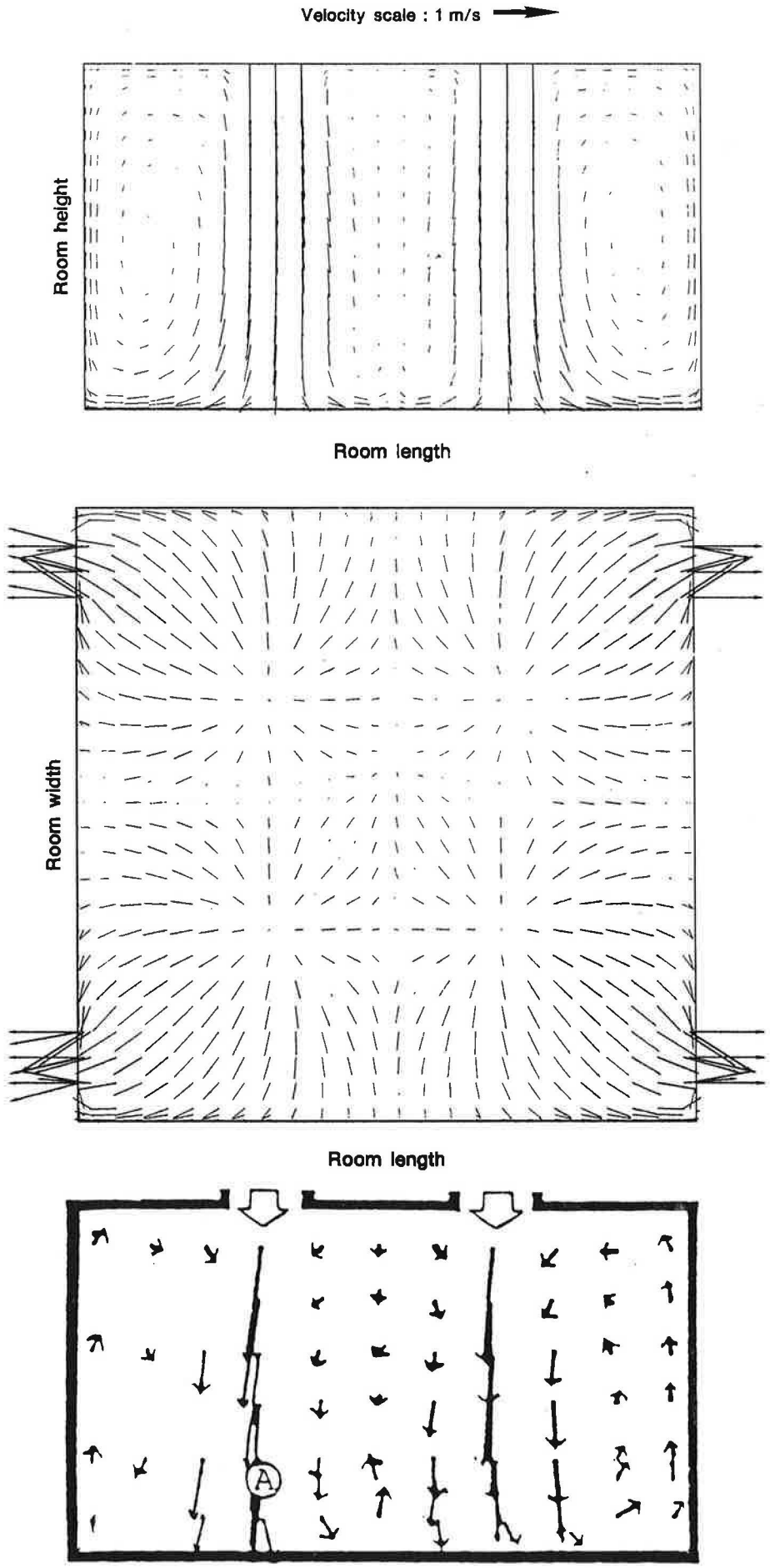

Fig 8 Predicted and experimental velocity vectors in the clean room
(a) Predicted for a vertical plane through supply opening
(b) Predicted for a horizontal plane 0.3m above the floor
(c) Experimental for a vertical plane through supply opening

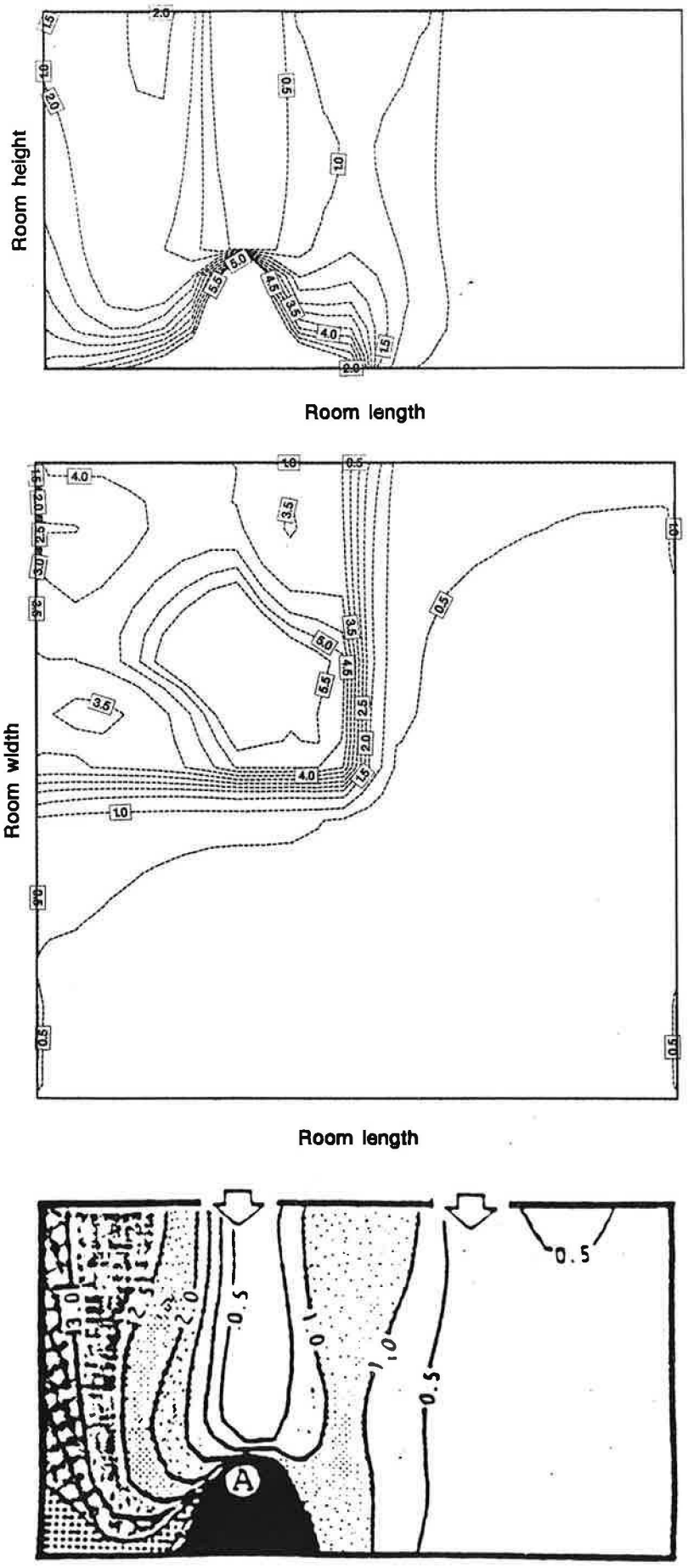

Fig 9 Predicted and experimental concentration contours in the clean room
(a) Predicted for a vertical plane through supply opening
(b) Predicted for a horizontal plane 0.3m above the floor
(c) Experimental for a vertical plane through supply opening

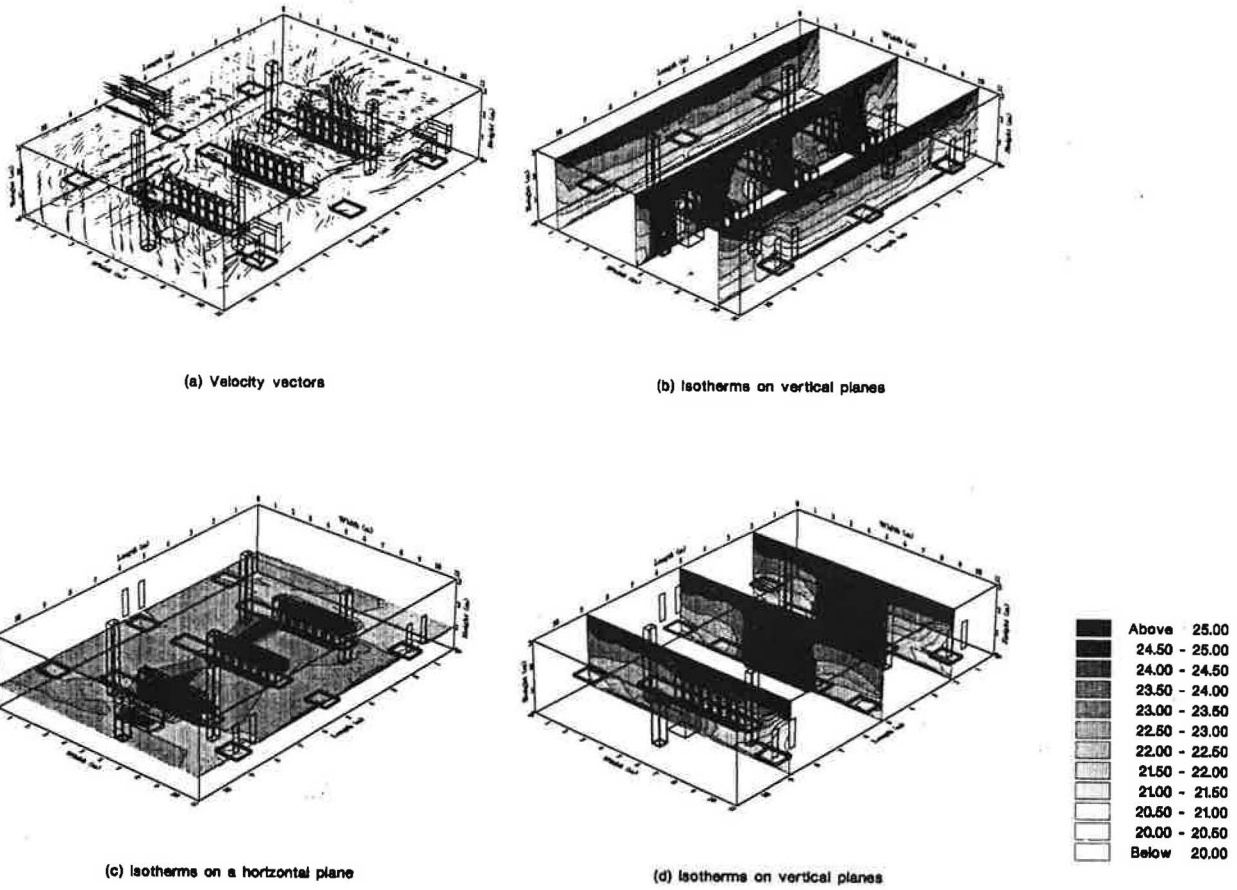

Fig 10 Predicted velocity vectors and isotherms in the classroom

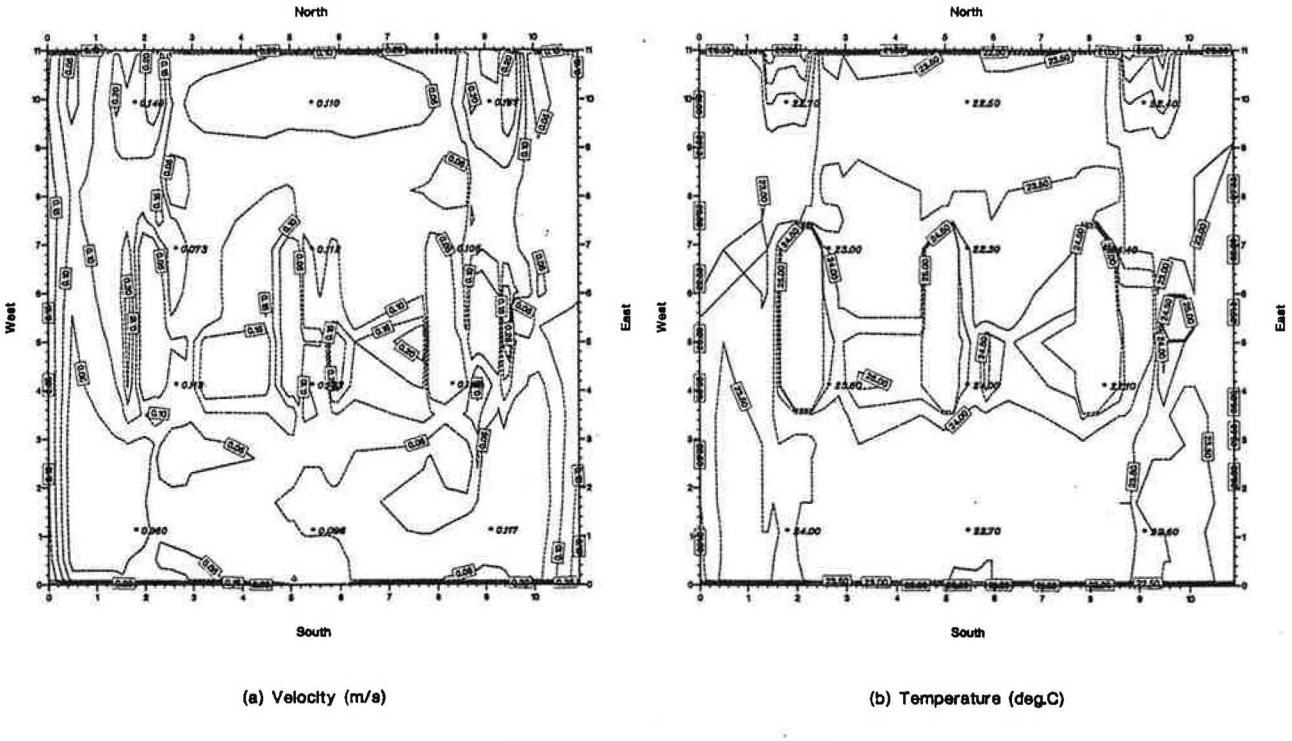

Fig 11 Comparison of predicted isovels and isotherms with measured velocities and temperatures (*) on a horizontal plane (0.9m above the floor) in the classroom

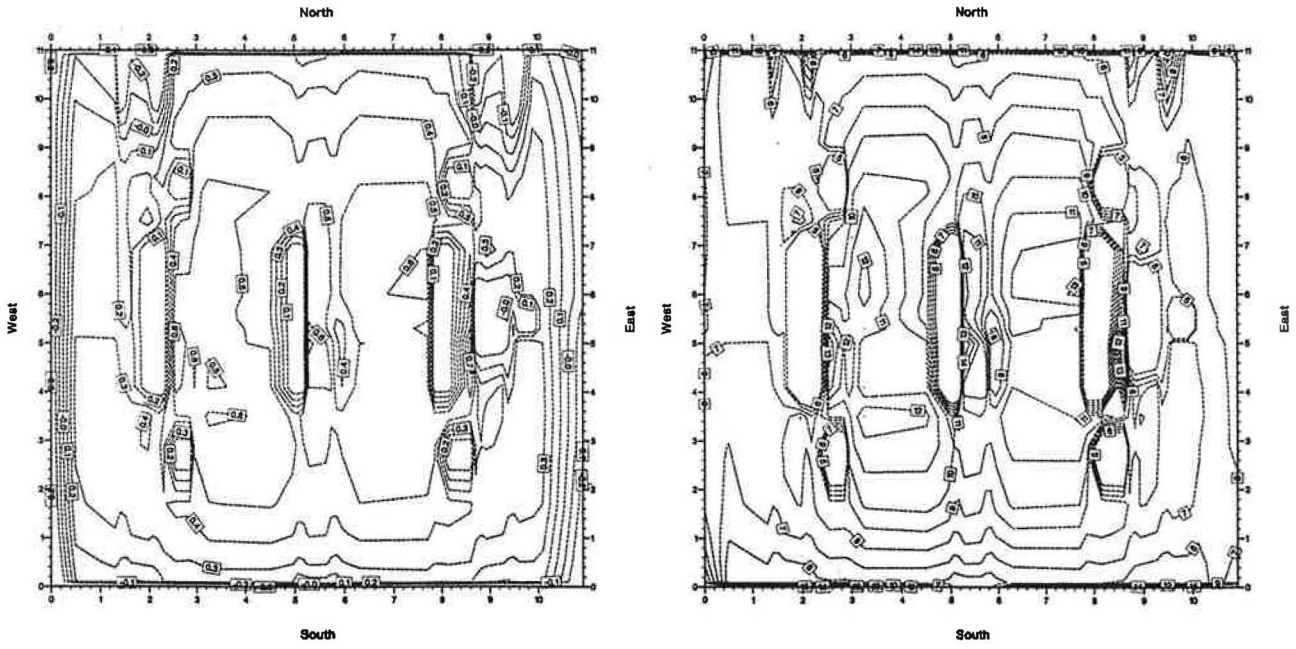

(a) Predicted mean vote

(b) Predicted percentage of dissatisfied (%)

Supply air: U = 0.356 m/s ; T = 19.9 deg.C

Fig 12 Contours of PMV and PPD on a horizontal plane (0.9m above the floor) in the classroom